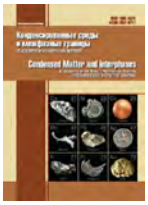

ISSN 1606-867X (Print)
ISSN 2687-0711 (Online)
Condensed Matter and Interphases
Kondensirovannye Sredy i Mezhfaznye Granitsy
https://journals.vsu.ru/kcmf/

Original articles

Research article
https://doi.org/10.17308/kcmf.2021.23/3435

Phase relations in the CuI-SbSI-SbI_3 composition range of the Cu–Sb–S–I quaternary system

P. R. Mammadli[1,2]✉, V. A. Gasymov[2], G. B. Dashdiyeva[3], D. M. Babanly[1,2]

[1]*Azerbaijan State Oil and Industry University, French - Azerbaijani University, 183 Nizami str., Baku AZ-1010, Azerbaijan*

[2]*Institute of Catalysis and Inorganic Chemistry of the Azerbaijan National Academy of Sciences, 113 H. Javid ave., Baku AZ-1143, Azerbaijan*

[3]*Baku Engineering University, 120 Hasan Aliyev str., Baku AZ-0102, Azerbaijan*

Abstract

The phase equilibria in the Cu-Sb-S-I quaternary system were studied by differential thermal analysis and X-ray phase analysis methods in the CuI-SbSI-SbI_3 concentration intervals. The boundary quasi-binary section CuI-SbSI, 2 internal polythermal sections of the phase diagram, as well as, the projection of the liquidus surface were constructed. Primary crystallisation areas of phases, types, and coordinates of non- and monovariant equilibria were determined. Limited areas of solid solutions based on the SbSI (β-phase) and high-temperature modifications of the CuI (α_1- and α_2- phases) were revealed in the system. The formation of the α_1 and α_2 phases is accompanied by a decrease in the temperatures of the polymorphic transitions of CuI and the establishment of metatectic (375^{0}C) and eutectoid (280^{0}C) reactions. It was also shown, that the system is characterised by the presence of a wide immiscibility region that covers a significant part of the liquidus surface of the CuI and SbSI based phases.

Keywords: Copper (I) iodide, Antimony iodide, Antimony sulfoiodide, Cu-Sb-S-I system, Phase diagram, Solid solutions

Acknowledgements: the work has been partially supported by the Science Development Foundation under the President of the Republic of Azerbaijan, a grant № EİF-BGM-4-RFTF-1/2017-21/11/4-M-12.

For citation: Mammadli P. R., Gasymov V. A., Dashdiyeva G. B., Babanly D. M. Phase relations in the CuI-SbSI-SbI_3 composition range of the Cu-Sb-S-I quaternary system. *Kondensirovannye sredy i mezhfaznye granitsy = Condensed Matter and Interphases*. 2021;23(2): 236–244. https://doi.org/10.17308/kcmf.2021.23/3435

Для цитирования: Маммадли П. Р., Гасымов В. А., Дашдиева Д. Б., Бабанлы Д. М. Фазовые равновесия в области составов CuI–SbSI–SbI_3 системы Cu–Sb–S–I. *Конденсированные среды и межфазные границы*. 2021;23(2): 236–244. https://doi.org/10.17308/kcmf.2021.23/3435

✉ Parvin Rovshan Mammadli, e-mail: parvin.mammadli@ufaz.az

1. Introduction

Copper-antimony chalcogenides and phases based on them are considered to be potential candidates for the preparation of environmentally friendly, low-cost functional materials possessing novel desired characteristics [1–3]. The majority of ternary Cu–Sb-sulphides are naturally occurring minerals that have been widely explored as valuable electronic materials displaying high photoelectric, photovoltaic, radiation detector, thermoelectric, etc. properties. Earth abundance and environmental compatibility of these substances highlight the recent advances of investigations on these materials [4–7].

As it is known, one of the ways to increase the efficiency of thermoelectric materials is to complicate their composition and crystal structure [8]. In this regard, Cu-Sb chalcohalides could be considered promising research objects in terms of the search and design of new eco-friendly functional materials. However, we could not find literary information about the phase equilibria of the Cu–Sb–S–I quaternary system. There is a literary report about the formation, crystal structure, and conductivity of the $Cu_5SbS_3I_2$ compound [9]. $Cu_5SbS_3I_2$ crystallises in the orthorhombic system, space group P*nnm* with the following lattice parameters a = 10.488(2), b = 12.619(2), c =7.316(1) Å, and Z = 4 [9]. Electric conductivity and dielectric parameters of the Cu–Sb–S–I glasses have been investigated in order to evaluate their practical importance in memory switching, electrical threshold, optical switching devices, and so forth [10].

The search and design of new complex functional materials require investigation of the respective phase diagrams. The information accumulated in phase diagrams of the corresponding systems is always helpful in materials science for the development of advanced materials [11–13].

Considering above mentioned facts, in terms of the search for new multicomponent phases, the concentration plane Cu_2S–CuI–SbI_3–Sb_2S_3 of the Cu–Sb–S–I quaternary system is of great interest. The present contribution is dedicated to the study of physicochemical interaction in the CuI–SbSI–SbI_3 (A) concentration area of the above-mentioned concentration plane.

Primary compounds of the system (A) possessing interesting functional properties have been studied in detail. Copper (I) iodide CuI is a non-poisonous, wide-gap semiconductor possessing stable p-type electrical conductivity at room temperature, fast-ionic conductivity at high temperatures, an unusually large temperature dependency, negative spin-orbit splitting, etc [14–16]. It has wide application in light-emitting diodes, solid-state dye-sensitised solar cells, high-performance thermoelectric elements, etc [17, 18]. Antimony triiodide SbI_3 has been intensively studied as a dopant in thermoelectric materials, as a potential material for radiation detectors, as cathodes in solid-state batteries, in high-resolution image microrecording, information storage, etc. [19–21]. SbSI exhibits important ferroelectricity, piezoelectricity, photoconduction, dielectric polarisation properties and is widely used in the fabrication of nanogenerators and nanosensors [22–25].

CuI melts at 606 °C without decomposition and has 3 modifications [26, 27]. The low-temperature γ-modification transforms to the β-phase at 369 °C. The β-CuI phase exists in a small temperature range (~ 10 K) and transforms into α-phase at 407 °C. SbI_3 melts at 172 °C [28] and crystallises to rhombohedral lattice [29]. SbSI melts congruently at 300 °C [22,30]. Three phases of SbSI have been reported: ferroelectric (T < 20 °C), antiferroelectric (20 °C < T <140 °C) and paraelectric (T < 140 °C) [31]. Both in the paraelectric and ferroelectric phases, SbSI crystallises in the orthorhombic structure [32, 33].

Crystallographic parameters of the constituent compounds of the system A are represented in Table 1.

CuI–SbI_3 and SbSI–SbI_3 boundary quasi-binary sections of the quasi-ternary CuI–SbSI–SbI_3 system have been investigated by [35–37], respectively. CuI–SbI_3 system forms a monotectic phase diagram. At the monotectic equilibrium temperature (~ 220 °C) the immiscibility region ranges within ~15–93 mol% SbI_3 concentration interval [35]. SbSI–SbI_3 quasi-binary section is characterised by a eutectic equilibrium at 160 °C [12, 30].

2. Experimental part

A CuI binary compound, as well as, antimony and iodine elementary components of the *Alfa*

Table 1. Crystal lattice types and parameters of the CuI, SbI_3, and SbSI compound

Compound, modification	Crystal lattice type and parameter, Å
LT–CuI	Cubic lattice; SpGr. F; *a* = 6.05844(3) Å [27]
HT1–CuI	Trigonal: SpGr. P3; *a* = 4.279±0.002; *c* = 7.168±0.007 (673 K) [34] Triqonal: SpGr. R-3; *a* = 4.29863(11); *c* = 21.4712(6) (603 K) [26] Triqonal: SpGr. R-3 *a* = 4.30571 (12); *c* = 21.4465(7) (608 K) [26]
HT2–CuI	Cubic: SpGr. F *a* = 6.16866(6) [27]
SbI_3	Rhombohedral: SpGr. ; *a* = 7.48; c = 20,90; Z = 6 [29]
SbSI	Orthorhombic: SpGr. P*nam*; *a* = 8.556(3); *b* = 10.186(4); *c* = 4.111(2); z = 4 [32] Orthorhombic: SpGr. P*na*2_1; *a* = 8.53; *b* = 10.14; *c* = 4.10 [33]

The symbols HT2, HT1, and LT indicate high, intermediate, and low-temperature modifications of CuI, respectively.

Aesar German brand (99.999 % purity) were used in the course of experimental studies.

Binary SbI_3 and ternary SbSI compounds were synthesised from the elemental components in evacuated (~10^{-2} Pa) silica ampoules followed by a specially designed method taking into account the high volatility of iodine and sulphur. The synthesis was performed in an inclined two-zone furnace, with the hot zone kept at a temperature 20–30 °C higher than the corresponding melting point of the synthesised compound, whereas the temperature of the cold zone was kept at about 130 °C. After the main portion of iodine and sulphur had reacted, the ampoules were relocated such that the products could melt at 230 °C (SbI_3) and 450 °C (SbSI). After stirring the homogeneous liquid at this temperature, the furnace gradually cooled. The purity and individuality of the obtained products were monitored using DTA and PXRD methods.

Two sets of samples (0.5 g by mass each) were prepared by co-melting of different proportions of the preliminarily synthesised compounds and CuI of the *Alfa Aesar* company. After melting, most of the alloys were annealed at about ~20–30 °C below the solidus temperature for ~1000 hours in order to achieve complete homogenisation.

The DTA and PXRD methods were used to monitor the purity and individuality of the synthesised compounds and to conduct experimental studies. DTA of the samples was carried out in evacuated quartz ampoules on a differential scanning calorimeter of the 404 F1 Pegasus System (NETZSCH). Results of measurements were processed using the NETZSCH Proteus Software. The accuracy of the temperature measurements was within ±2 °C. X-ray analysis of the annealed alloys was carried out at room temperature on the Bruker D2 PHASER diffractometer with Cu$K\alpha_1$ radiation. The diffraction patterns were indexed using the Topas 4.2 Software (Bruker).

3. Results and discussion

A co-analysis of experimental results together with the literature data regarding boundary binary systems helped us to obtain the full description of phase equilibria in the CuI-SbSI-SbI_3 concentration triangle.

3.1. CuI–SbSI boundary quasi-binary system

The powder X-ray diffraction patterns of the thermally treated CuI–SbSI alloys are given in Fig. 1. As can be seen, diffraction patterns of samples in the full composition range consist of the diffraction peaks of the SbSI and low-temperature modification of CuI.

The *T-x* phase diagram of the system (Fig. 2) was constructed using DTA results (Table 2). Note that, α_1 and α_2 are solid solutions based on the HT1 – CuI and HT2 – CuI respectively, and β – is a solid solution based on SbSI.

The system is quasi-binary and forms a eutectic phase diagram. Eutectics has a ~ 45 mol% SbSI composition and crystallises at 327 °C by the reaction:

$L \rightarrow \alpha_2 + \beta$.

The formation of α_1 and α_2 solid solution areas based on the high-temperature modifications of CuI is accompanied by a decrease in temperature of its' both phase transformations and these phase transitions occur by metatectic and eutectoid reactions.

Isotherms corresponding to the 375 and 280 °C temperatures on the phase diagram, reflect metatectic

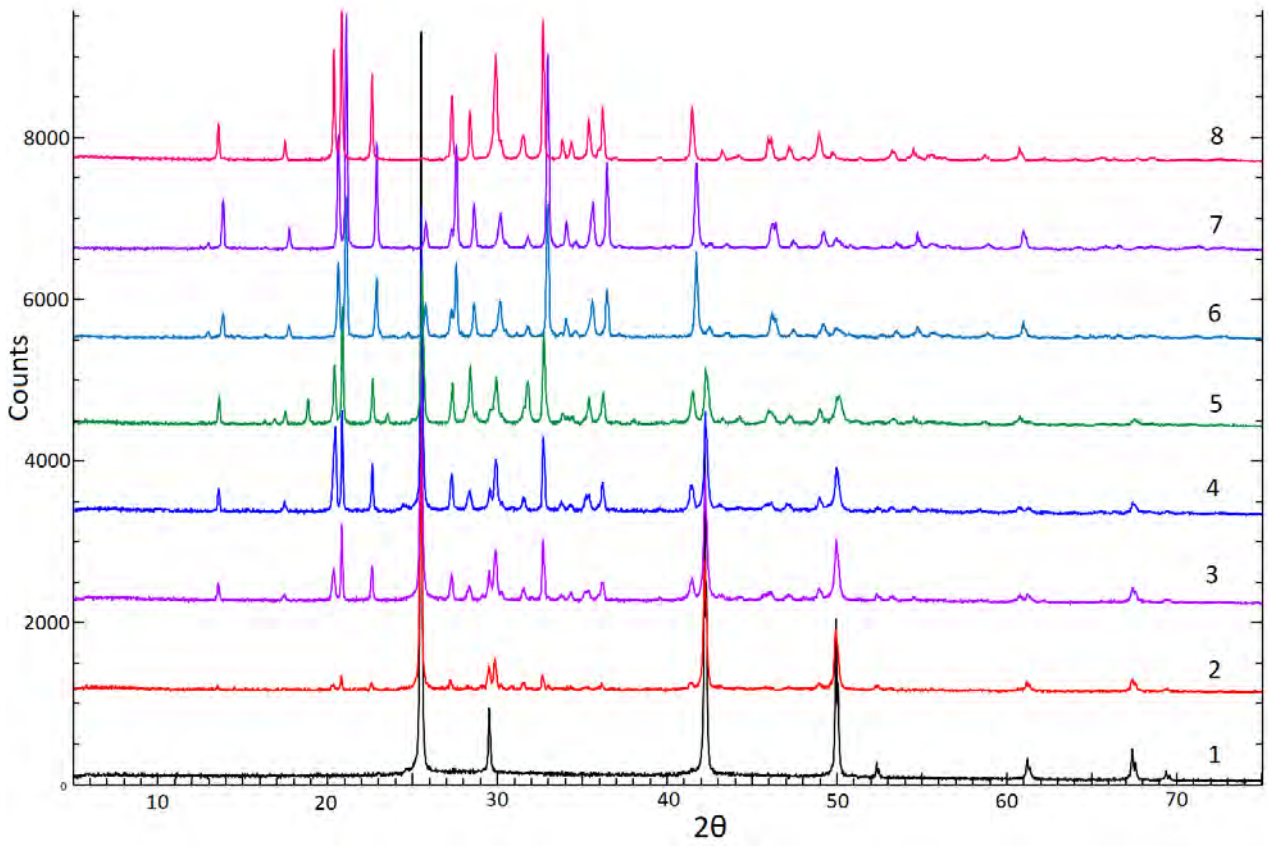

Fig. 1. X-ray images of different alloys of the CuI–SbSI system: *1* – CuI, *2* – 10 mol% CuI, *3* – 20 mol% CuI, *4* – 40 mol% CuI, *5* – 60 mol% CuI; *6* – 80 mol% CuI; *7* – 90 mol% CuI; *8* – SbSI

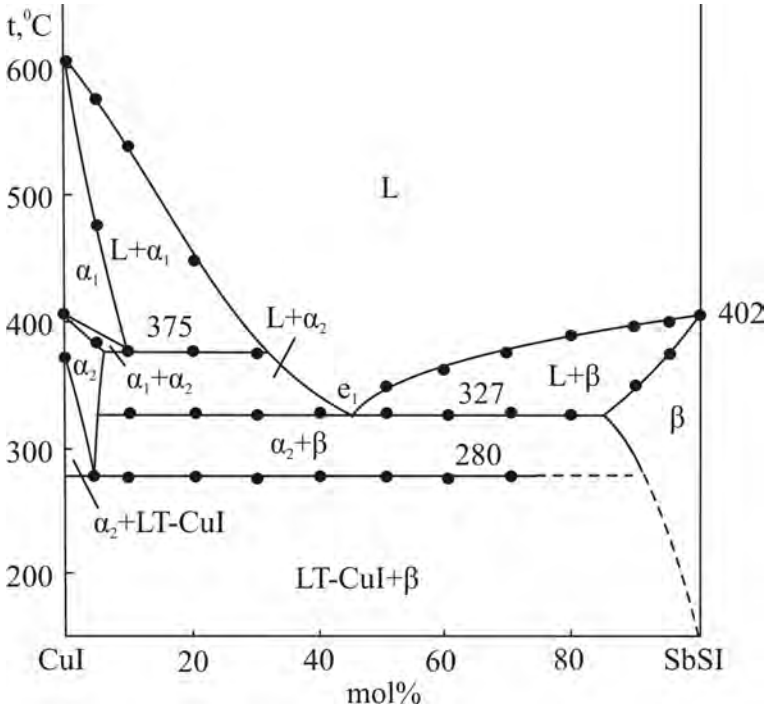

Fig. 2. *T-x* phase diagram of the CuI–SbSI system

Table 2. DTA results of the CuI–SbSI system

Composition, mol% SbSI	Thermal effects, °C	
	Isothermal	Polythermal
0 (pure CuI)	369; 407; 606	–
5	280; 385	470–573
10	280; 325; 375	375–534
20	282; 327; 373	373–455
30	280; 328; 376	–
40	278; 327	–
50	280; 327	327–343
60	280; 328	328–360
70	279; 327	327–375
80	327	327–382
90	–	352–394
95	–	380–398
100 (pure SbI_3)	402	–

$\alpha_1 \leftrightarrow L + \alpha_2$

and eutectoid

$\alpha_2 \leftrightarrow$ LT-CuI + β.

equilibriums, respectively.

The homogeneity region of the β-phase based on SbSI is maximum (~15 mol%) at the eutectic temperature (Fig. 2). Moreover, reflection angles belonging to LT-CuI and SbSI phases on powder diffractograms are fully compatible with appropriate pure compounds. It shows that the mutual solubility of these compounds is negligible at room temperature. Therefore, in Fig. 2, the decomposition curve of the β-phase is extrapolated to the SbSI compound.

3.2. Projection of the liquidus surface (Fig. 3)

Fig. 3 represents a projection of the *T-x-y* diagram of the CuI–SbSI–SbI_3 system, where liquidus isotherms are given in blue. The liquidus surface consists of three fields describing the primary crystallisation of the α_1 (α_2), β-phases, and SbI_3. The latter occupies a small region near the appropriate corner of the concentration triangle.

Primary crystallisation surfaces of phases are limited by a number of monovariant equilibrium curves and non-variant equilibrium points (Table 3).

The L_1+L_2 immiscibility region in the CuI-SbI_3 boundary system sharply penetrates into the concentration triangle and covers part of

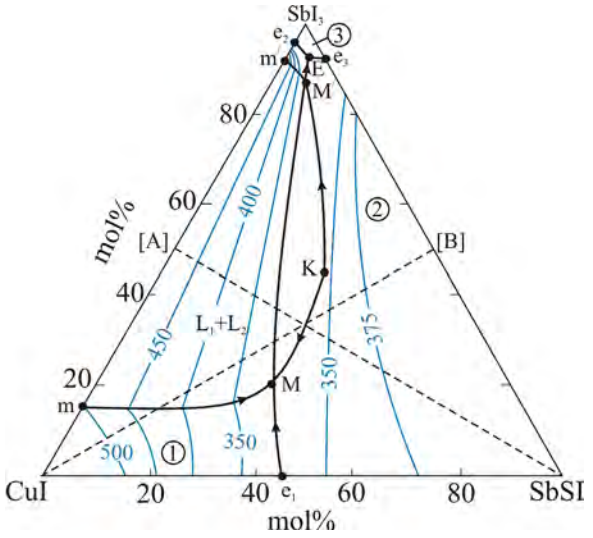

Fig. 3. Projection of the liquidus surface of the system CuI–SbSI–SbI_3. Primary crystallisation fields: *1* – α_1 (α_2); *2* – β phase; *3* – SbI_3. Dotted lines are studied polythermal sections

the liquidus area of the β phase by crossing the eutectic curve from the point e_1. Consequently, the $L \leftrightarrow \alpha_2 + \beta$ monovariant eutectic equilibrium shifts to the $L_1 \leftrightarrow L_2 + \alpha_2 + \beta$ nonvariant monotectic equilibrium (Fig. 3, Table 1 – MM′ conjugate pair). K is the critical point of stratification and has a temperature of ~350 °C.

Crystallisation across the whole system ends at 165 °C by nonvariant eutectic (E) reaction.

3.3. Polythermal sections

The CuI–[B] (Fig. 4) and [A]–SbSI (Fig. 5) polythermal sections of the phase diagram of the CuI–SbSI–SbI_3 ternary system are given below and analysed in context with the projection of the liquidus surface of the system. Here, [A] and [B] are 1:1 mix ratios of the constituent compounds of the CuI–SbI_3 and SbSI–SbI_3 side binary systems, consequently.

The system CuI-[B] (Fig. 4). This section passes through the initial crystallisation areas of the α_1 (α_2) and β-phases and the immiscibility area in the ~ 30–70 mol% CuI concentration range. Crystallisation in the compositions rich in CuI initially continues by the monovariant monotectic $L_1 \leftrightarrow L_2 + \alpha_1$ reaction and leads to the formation of the $L_1 + L_2 + \alpha_1$ three-phase area. At 377 °C this phase field is replaced by the $L_1 + L_2 + \alpha_1$ three-phase area as a result of the $\alpha_1 \leftrightarrow \alpha_2$ phase transition. Crystallisation in the 20–40 mol% CuI

Table 3. Non- and monovariant equilibria of the CuI–SbSI–SbI_3 system

Point in Fig. 3	Equilibrium	Composition, mol%		Temperature, °C
		SbSI	SbI_3	
e_1	$L \leftrightarrow \alpha_2 + \beta$	45	–	327
e_2	$L \leftrightarrow$ LT-CuI + SbI_3	–	97	168
e_3	$L \leftrightarrow$ SbSI + SbI_3	7	93	167
m (m′)	$L_1 \leftrightarrow L_2 + \alpha_1$	–	15 (93)	493
M (M′)	$L_1 \leftrightarrow L_2 + \alpha_2 + \beta$	34 (6)	20 (87)	318
E	$L \leftrightarrow$ LT-CuI + β +SbI_3	–	–	165
Curve in Fig. 3	Equilibrium	Temperature interval, °C		
mM (m′M′)	$L_1 \leftrightarrow L_2 + \alpha_1$	493–318		
KM (KM′)	$L_1 \leftrightarrow L_2 + \beta$	340–318		
e_1M	$L \leftrightarrow \alpha_2 + \beta$	327–318		
M′E	$L \leftrightarrow \alpha_2$ (LT-CuI) + β	318–165		
e_2E	$L \leftrightarrow$ LT-CuI + SbI_3	168–165		
e_3E	$L \leftrightarrow \beta + SbI_3$	167–165		

composition range continues by the $L_1 \leftrightarrow L_2 + \beta$ monotectic scheme and forms the $L_1 + L_2 + \beta$ phase area. Horizontal line at 318 °C belongs to the $L_1 \leftrightarrow L_2 + \alpha_2 + \beta$ nonvariant monotectic reaction (Table 2). After this reaction, the $L_2 + \alpha_2 + \beta$ three-phase area forms in the system. At 280 °C, the $\alpha_2 \leftrightarrow$ LT-CuI phase transitions occur and the latter phase area passes to the $L_2 + \beta$ + LT-CuI.

Crystallisation of all samples along the system ends at 165 °C by the nonvariant eutectic reaction (E) and the β + LT-CuI + SbI_3 three-phase mixture forms.

The system [A]–SbSI (Fig. 5). This polythermal section is situated in the $L_1 + L_2$ immiscibility area at the 0–40 mol% SbSI composition range and crystallisation processes occur by monotectic reactions (Fig. 3, mMK and m′M′K′ conjugate curves). In the course of those processes the $L_1 + L_2 + \alpha_1$, $L_1 + L_2 + \alpha_2$, $L_1 + L_2$ + LT-CuI and $L_1 + L_2 + \beta$ three-phase areas are formed. In the alloys rich in SbSI, crystallisation of this compound initially occurs from the liquid solution, then continues by the $L_1 \leftrightarrow L_2$ + SbSI monotectic scheme. All alloys are exposed to the nonvariant monotectic

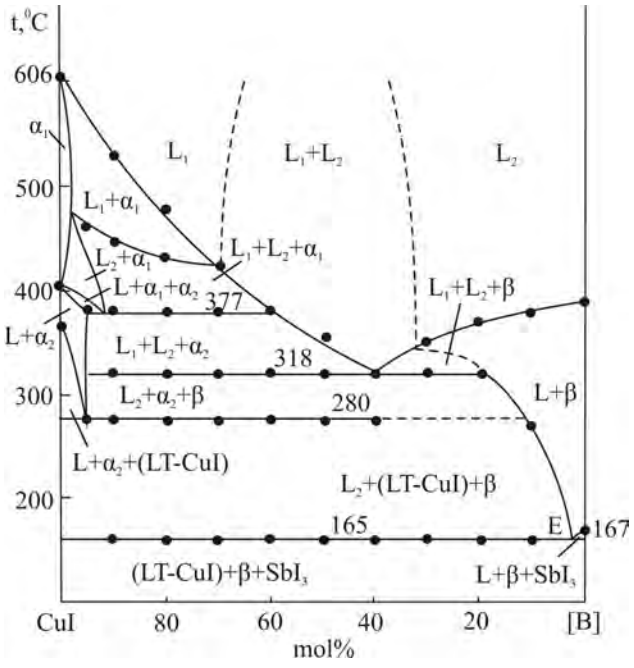

Fig. 4. *T-x* phase diagram of the system CuI–[B]

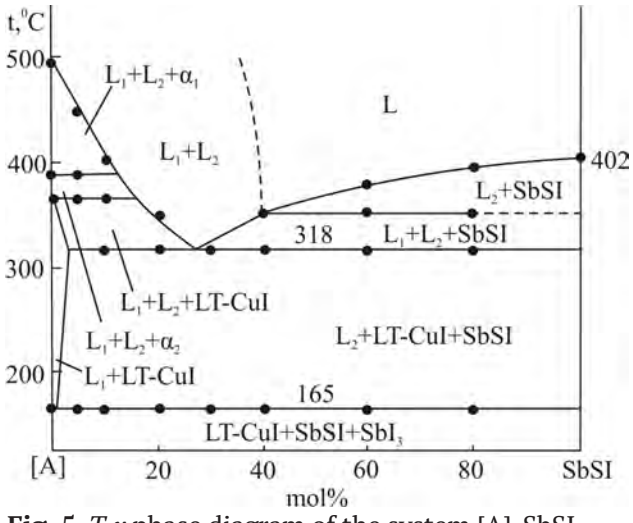

Fig. 5. *T-x* phase diagram of the system [A]-SbSI

reaction (m) at 318 ^{0}C and fully crystallise by the nonvariant eutectic reaction at 165 °C.

Fig. 6 shows the DTA heating curves of selected annealed samples along the boundary quasi-binary system CuI–SbSI and the above-mentioned internal sections. Comparison of these curves with the corresponding *T-x* diagrams (Fig. 2, 4, 5), the projection of the liquidus surface (Fig. 3) and the table shows that they accurately reflect the character and temperatures of the processes occurring in the system.

4. Conclusion

The phase equilibria in the CuI-SbSI-SbI_3 composition range of the Cu-Sb-S-I quaternary system have been studied for the first time. Several polythermal sections of the phase diagram including the CuI-SbSI boundary system and *T-x-y* projection of the liquidus surface of the system was obtained by co-analysis of experimental results along with the literature data on boundary binary systems. It was determined that there are limited solid solutions based on SbSI (β-phases) and HT-CuI (α_1- and α_2-phases) and the system is characterised by the formation of a large immiscibility area. The types and coordinates of non- and monovariant equilibria, as well as, primary crystallisation areas of phases were determined.

Contribution of the authors

P. R. Mammadli – experimental investigations, writing original draft, making conclusions. V. A. Gasymov – powder X-ray analysis. G. B. Dashdiyeva – research concept, methodology development. D. M. Babanly – scientific management, review and editing.

Conflict of interests

The author declares that they have no known competing financial interests or personal relationships that could have appeared to influence the work reported in this paper.

References

1. Ivanov-Shhic A. K., Murin. I. V. *Ionika tverdogo tela. V 2-h tomah* [Ionic Solid State (in 2 vol.)]. St. Petersburg: Izd-vo S.- Peterb. un-ta Publ. 2000;1: 616. (In Russ.)

2. Babanly M. B., Mashadiyeva L. F., Babanly D. M., Imamaliyeva S. Z., Tagiyev D. B., Yusibov Y. A.. Some issues of complex studies of phase equilibria and thermodynamic properties in ternary chalcogenide systems involving Emf measurements. *Russian Journal of Inorganic Chemistry*. 2019;64(13): 1649–1672. https://doi.org/10.1134/s0036023619130035

3. Peccerillo E., Durose K. Copper–antimony and copper–bismuth chalcogenides—Research opportunities and review for solar photovoltaics. *MRS Energy & Sustainability.* 2018;5(9): 1–59. https://doi.org/10.1557/mre.2018.10

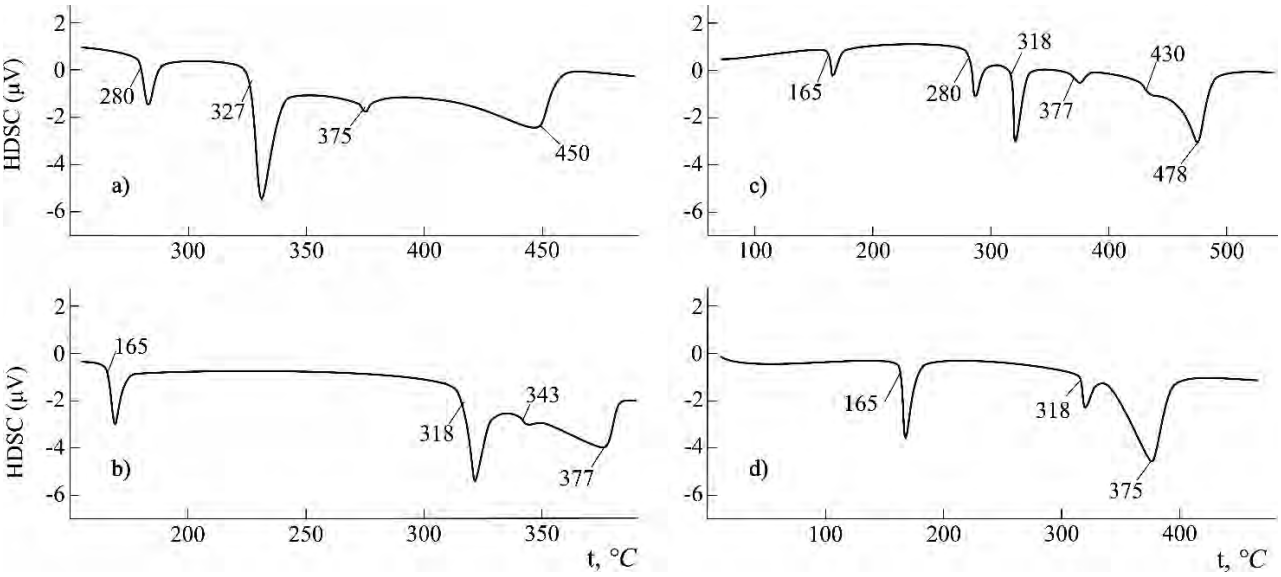

Fig.6. DTA heating curves of some samples: alloy of composition 20 mol% SbSI of the CuI–SbSI system (a); alloys with compositions 30 (b) and 80 mol% CuI (c) along the section CuI–[B]; and 60 mol% SbSI (d) along the section [A] – SbSI

4. Loranca-Ramos F. E., Diliegros-Godines C. J., Silva-González R., Pal M. Structural, optical and electrical properties of copper antimony sulfide thin films grown by a citrate-assisted single chemical bath deposition. *Applied Surface Science*. 2018;427: 1099–1106. https://doi.org/10.1016/j.apsusc.2017.08.027

5. Chetty R., Bali A., Mallik R. C. Tetrahedrites as thermoelectric materials: an overview. *Journal of Materials Chemistry C*. 2015;3(48): 12364–12378. https://doi.org/10.1039/C5TC02537K

6. Van Embden J., Latham K., Duffy N. W., Tachibana Y. Near-infrared absorbing $Cu_{12}Sb_4S_{13,}$ and Cu_3SbS_4 nanocrystals: Synthesis, characterization, and photoelectrochemistry. *Journal of the American Chemical Society*. 2013;135(31): 11562–11571. https://doi.org/10.1021/ja402702x

7. Lu X., Morelli D. T., Xia Y., Zhou F., Ozolins V., Chi H., Zhou X., Uher C. High performance thermoelectricity in earth-abundant compounds based on natural mineral tetrahedrites. *Advanced Energy Materials*. 2013;3(3): 342–348. https://doi.org/10.1002/aenm.201200650

8. Ioffe A. F. *Semiconductor thermoelements and thermoelectric cooling*. London: Infosearch Ltd; 1957.

9. Pfitzner A. $(CuI)_2Cu_3SbS_3$: copper iodide as solid solvent for thiometalate ions. *Chemistry – A European Journal*. 1997;3(12): 2032–2038. https://doi.org/10.1002/chem.19970031218

10. Rubish V. M. Electric and dielectric properties of glasses of Cu-Sb-S-I system. *Semiconductor Physics, Quantum electronics, and Optoelectronics*. 2003;6(1): 76–80. http://dspace.nbuv.gov.ua/handle/123456789/117961

11. Babanly M. B., Chulkov E. V., Aliev Z. S., Shevelkov A. V., Amiraslanov I. R. Phase diagrams in materials science of topological insulators based on metal chalkogenides. *Russian Journal of Inorganic Chemistry*. 2017;62(13): 1703–1729. https://doi.org/10.1134/S0036023617130034

12. Aliyev Z. S., Musayeva S. S., Babanly M. B. The phase relationships in the Sb-S-I system and thermodynamic properties of the SbSI. *Journal of Phase Equilibria and Diffusion*. 2017;38(12): 887–896. https://doi.org/10.1007/s11669-017-0601-4

13. Babanly D. M., Tagiyev D. B. Physicochemical aspects of ternary and complex phases development based on thallium chalcohalides. *Chemical Problem*. 2018;16 (2): 153–177. https://doi.org/10.32737/2221-8688-2018-2-153-177

14. Koyasu S., Umezawa N., Yamaguchi A., Miyauchi. M. Optical properties of single crystalline copper iodide with native defects: Experimental and density functional theoretical investigation. *Journal of Applied Physics*. 2019;125(11): 115101. https://doi.org/10.1063/1.5082865

15. Grundmann M., Schein F-L., Lorenz M., Böntgen T., Lenzner J., Wenckstern H. Cuprous iodide – a p-type transparent semiconductor: history and novel applications. *Physica Status Solidi A*. 2013;210(9): 1671–1703. https://doi.org/10.1002/pssa.201329349

16. Amalina M. N., Azilawati Y., Rasheid N. A., Rusop M. The properties of copper (I) iodide (CuI) thin films prepared by mister atomizer at different doping concentration. *Procedia Engineering*. 2013;56: 731 – 736. https://doi.org/10.1016/j.proeng.2013.03.186

17. Perera V. P. S., Tennakone K. Recombination processes in dye-sensitized solid-state solar cells with CuI as the hole collector. *Solar Energy Materials and Solar Cells*. 2003;79(2): 249–255. https://doi.org/10.1016/S0927-0248(03)00103-X

18. Christians J. A., Fung R. C. M., Kamat P. V. An inorganic hole conductor for organo-lead halide perovskite solar cells. Improved hole conductivity with copper iodide. *Journal of the American Chemical Society*. 2014;136(2): 758–764. https://doi.org/10.1021/ja411014k

19. Onodera T., Baba K., Hitomi K. Evaluation of antimony tri-iodide crystals for radiation detectors. *Science and Technology of Nuclear Installations*. 2018;1532742: 1–7. https://doi.org/10.1155/2018/1532742

20. Mohan D. B., Philip A., Sunandana C. S. Iodization of antimony thin films: XRD, SEM, and optical studies of nanostructured SbI_3. *Vacuum*. 2008;82(6): 561–565. https://doi.org/10.1016/j.vacuum.2007.08.014

21. Kępińska M., Starczewska A., Bednarczyk I., Szala J., Szperlich P., Mistewicz K. Fabrication and characterisation of SbI_3-opal structures. *Materials Letters*. 2014;130: 17–20. http://dx.doi.org/10.1016/j.matlet.2014.05.063

22. Toron B., Szperlich P., Koziol M. SbSI composites based on epoxy resin and cellulose for energy harvesting and sensors - the influence of SbSI nanowires conglomeration on piezoelectric properties. *Materials*. 2020;13(4): 902. https://doi.org/10.3390/ma13040902

23. Purusothaman Y., Alluri N. R., Chandrasekhar A., Kim S. J. Photoactive piezoelectric energy harvester driven by antimony sulfoiodide (SbSI): A $A_VB_{VI}C_{VII}$ class ferroelectric-semiconductor compound. *Nano Energy*. 2018;50: 256–265. https://doi.org/10.1016/j.nanoen.2018.05.058

24. Jesionek M., Toron B., Szperlich P., Binias W., Binias D., Rabiej S., Starczewska A., Nowak M., Kępińska M., Dec J. Fabrication of a new PVDF/SbSI nanowire composite for smart wearable textile. *Polymer*. 2019;180: 121729. https://doi.org/10.1016/j.polymer.2019.121729

25. Szperlich P., Toron B. An ultrasonic fabrication method for epoxy resin/SbSI nanowire composites, and their application in nanosensors and nanogenerators. *Polymers*. 2019;11(3): 479. https://doi.org/10.3390/polym11030479

26. Shan Y., Li G., Tian G., Han J., Wang Ch., Liu Sh., Du H., Yang Y. Description of the phase transitions of cuprous iodide. *Journal of Alloys and Compounds*. 2009;477(1-2): 403–406. https://doi.org/10.1016/j.jallcom.2008.10.026

27. Yashima M., Xu Q., Yoshiasa A., Wada S. Crystal structure, electron density, and diffusion path of the fast-ion conductor copper iodide CuI. *Journal of Materials Chemistry*. 2006;16(45): 4393–4396. https://doi.org/10.1039/B610127E

28. Rolsten R. F. *Iodide metals and metal iodides*. New York: John Wiley and Sons; 1961.

29. Trotter J., Zobel T. The crystal structure of SbI_3 and BiI_3. *Zeitschrift fur Kristallographie - Crystalline Materials*. 1966;123(1-6): 67–72. https://doi.org/10.1524/zkri.1966.123.16.67

30. Ryazantsev T. A., Varekha L. M., Popovkin B. A., Lyakhovitskaya V. A., Novoselova A. V. *P-T-x* phase diagram of the SbI_3-Sb_2S_3 system. *Izv. Akad. Nauk. Neorg. Mater*. 1969;5(7): 2196–2197. (in Russ.)

31. Audzijonis A., Sereika R., Zaltauskas R. Antiferroelectric phase transition in SbSI and SbSeI crystals. *Solid State Commun*. 2008;147(3-4): 88–89. https://doi.org/10.1016/j.ssc.2008.05.008

32. Lukaszewicz K., Pietraszko A., Stepen' Damm Yu, Kajokas A. Crystal structure and phase transitions of the ferroelectric antimony sulfoiodide SbSI. Part II. Crystal structure of SbSI, in Phases I, II, and III. *Polish Journal of Chemistry*. 1997;71: 1852–1857.

33. Itoh K., Matsunaga H. A Study of the crystal structure in ferroelectric SbSI. *Zeitschrift für Kristallographie - Crystalline Materials*. 1980;152(1-4): 309–315. https://doi.org/10.1524/zkri.1980.152.14.309

34. Sakuma T. Crystal structure of β-CuI. *Journal of the Physical Society of Japan*. 1988;57(2): 565–569. https://doi.org/10.1143/JPSJ.57.565

35. Mammadli P. R. Physico-chemical interaction of the copper and antimony iodides. *Azerbaijan Chemical Journal*. 2021;1: 43–49. https://doi.org/10.32737/0005-2531-2021-1-43-47

Information about the authors

Parvin R. Mammadli, PhD student in Chemistry, a Chemistry Teacher at French-Azerbaijani University, Azerbaijan State Oil and Industry University, Baku, Azerbaijan; e-mail: parvin.mammadli@ufaz.az. ORCID iD: https://orcid.org/0000-0002-8062-1485.

Vagif A. Gasymov, PhD in Chemistry, Assistance Professor, Institute of Catalysis and Inorganic Chemistry, Azerbaijan National Academy of Sciences, Baku, Azerbaijan; e-mail: v-gasymov@rambler.ru. ORCID iD: https://orcid.org/0000-0001-6233-5840.

Ganira B. Dashdiyeva, PhD in Chemistry, Chemistry Teacher, Baku Engineering University, Baku, Azerbaijan; e-mail: ganira.dasdiyeva@mail.ru.

Dunya M. Babanly, DSc in Chemistry, Coordinator of the Chemistry Department, Lecturer at French-Azerbaijani University, Senior Researcher of the Institute of Catalysis and Inorganic Chemistry, Azerbaijan National Academy of Sciences, Baku, Azerbaijan; e-mail: dunya.babanly@ufaz.az. ORCID iD: https://orcid.org/0000-0002-8330-7854 .

Received 16 February 2021; Approved after reviewing 9 April 2021; Accepted 15 May 2021; Published online 25 June 2021.

Edited and proofread by Simon Cox